Dalton Transactions

PAPER

View Article Online
View Journal | View Issue

Cite this: *Dalton Trans.*, 2015, **44**, 8238

A study on the thermal conversion of scheelite-type ABO_4 into perovskite-type $AB(O,N)_3$†

Wenjie Li,[a] Duan Li,[b] Xin Gao,[b] Aleksander Gurlo,[c] Stefan Zander,[d] Philip Jones,[e] Alexandra Navrotsky,[e] Zhijian Shen,[b] Ralf Riedel[a] and Emanuel Ionescu*[a]

Received 17th February 2015,
Accepted 27th March 2015

DOI: 10.1039/c5dt00711a

www.rsc.org/dalton

Phase-pure scheelite $AMoO_4$ and AWO_4 (A = Ba, Sr, Ca) were thermally treated under an ammonia atmosphere at 400 to 900 °C. $SrMoO_4$ and $SrWO_4$ were shown to convert into cubic perovskite $SrMoO_2N$ and $SrWO_{1.5}N_{1.5}$, at 700 °C and 900 °C respectively, and to form metastable intermediate phases (scheelite $SrMoO_{4-x}N_x$ and $SrWO_{4-x}N_x$), as revealed by X-ray diffraction (XRD), elemental analysis and FTIR spectroscopy. High-temperature oxide melt solution calorimetry reveals that the enthalpy of formation for $SrM(O,N)_3$ (M = Mo, W) perovskites is less negative than that of the corresponding scheelite oxides, though the conversion of the scheelite oxides into perovskite oxynitrides is thermodynamically favorable at moderate temperatures. The reaction of $BaMO_4$ with ammonia leads to the formation of rhombohedral $Ba_3M_2(O,N)_8$ and the corresponding binary metal nitrides Mo_3N_2 and $W_{4.6}N_4$; similar behavior was observed for $CaMO_4$, which converted upon ammonolysis into individual oxides and nitrides. Thus, $BaMO_4$ and $CaMO_4$ were shown to not provide access to perovskite oxynitrides. The influence of the starting scheelite oxide precursor, the structure distortion and the degree of covalency of the B-site-N bond are discussed within the context of the formability of perovskite oxynitrides.

1 Introduction

Perovskite oxynitrides $AB(O,N)_3$ are typically synthesized *via* ammonolysis of oxide precursors; thus they can be formally represented as nitrogen-substituted perovskite-type oxides,[1,2] which are an emerging class of materials suitable for novel applications in the fields of energy conversion, storage, non-toxic pigments, dielectrics, *etc.*[3]

Most perovskite-type oxynitrides are synthesized *via* conversion of scheelite-type ABO_4 and pyrochlore-type $A_2B_2O_7$ upon thermal treatment under an ammonia atmosphere. However, not all scheelite- and pyrochlore-type oxides are able to afford perovskite oxynitrides. For example, pyrochlore-type $La_2Zr_2O_7$ as well as scheelite-type $EuMO_4$ (M = Nb and Ta) and $SrMoO_4$ provide perovskite-type $LaZrO_2N$[4] as well as $EuMO_2N$[5] and $SrMoO_2N$,[6] respectively, whereas other precursor oxides such as scheelite-type $ATaO_4$ (A = Nd, Sm, Gd, Dy) and $A_2W_2O_9$ (A = Pr, Nd, Sm, Gd, Dy) convert upon ammonolysis into pyrochlore-type $A_2Ta_2O_5N_2$,[7] and scheelite-type AWO_3N,[8] respectively.

According to our previous work, only a limited number of perovskite-type oxynitrides are formable.[9] For instance, $SrMoO_2N$, $SrWO_2N$, $CaMoO_2N$ and $CaWO_2N$ appear to be feasible, while $BaMoO_2N$ and $BaWO_2N$ are not stable in the perovskite-type structure. Although perovskite-type $SrMo(O,N)_3$, $SrW(O,N)_3$ and $CaMo(O,N)_3$ [6,10–14] have been reported in the literature (consistent with our prediction based on tolerance and octahedral factors),[9] details of the structure evolution of the oxides into perovskite-type oxynitrides are scarce. Furthermore, the existence of perovskite-type $BaMo(O,N)_3$ is questionable;[11,12] whereas perovskite-type $BaW(O,N)_3$ and $CaW(O,N)_3$ have not yet been synthesized.

2 Experimental methods

2.1 Synthesis

Scheelite-type oxide precursors (*i.e.*, $SrMoO_4$, $SrWO_4$, $BaMoO_4$, $BaWO_4$, $CaMoO_4$ and $CaWO_4$) were synthesized *via* solvothermal methods. Thus, $Sr(NO_3)_2$ (Sigma-Aldrich, >99.0%),

[a]*Fachbereich Material- und Geowissenschaften Technische Universität Darmstadt, 64287 Darmstadt, Germany. E-mail: ionescu@materials.tu-darmstadt.de; Fax: +49 (0)6151 16 6346; Tel: +49 (0)6151 16 6342*
[b]*Department of Materials and Environmental Chemistry, Arrhenius Laboratory, Stockholm University, S-106 91 Stockholm, Sweden*
[c]*Fachgebiet Keramische Werkstoffe, Institut für Werkstoffwissenschaften und –technologien Fakultät III Prozesswissenschaften, Technische Universität Berlin, Hardenbergstraße 40, 10623 Berlin, Germany*
[d]*Helmholtz-Zentrum Berlin für Materialien und Energie, Department of Crystallography, Hahn-Meitner-Platz 1, 14109 Berlin, Germany*
[e]*Peter A. Rock Thermochemistry Laboratory and NEATORU, University of California Davis, Davis, CA 95616-8779, USA*

†Electronic supplementary information (ESI) available: XRD, FTIR, lattice parameters and the phase composition obtained by Rietveld refinement, elemental analysis and the enthalpies of formation results as well as Gibbs free energy calculation. See DOI: 10.1039/c5dt00711a

$Ba(NO_3)_2$ (Sigma-Aldrich, >99.0%) or $Ca(NO_3)_2{\cdot}4H_2O$ (Sigma-Aldrich, >99.0%) was mixed in an equimolar ratio with $Na_2MoO_4{\cdot}4H_2O$ (Sigma-Aldrich, >99.5%) or $Na_2WO_4{\cdot}4H_2O$ (Sigma-Aldrich, >99.5%) in ethylenediamine (FLUKA, >99.5%) under vigorous stirring. Subsequently, the reaction mixture was transferred into an autoclave with Teflon lining and heated at 200 °C for 24 h. The resulting mixture was rinsed 5 times with deionized water and ethanol alternately. Centrifugation and drying at 60 °C overnight led to the powdered scheelite-type oxides.

The resulting oxides were ground to fine powders (grain size < 500 nm) and placed in a silica crucible. The thermal treatments were carried out in flowing ammonia at temperatures between 400 and 900 °C for 4–24 h. The Schlenk system used for thermal ammonolysis is specifically limited to small batch sizes (about 0.3–0.5 g) to maximize exposure to flowing NH_3 and thus the product homogeneity.

2.2 Sample characterization

The crystalline phase composition of the as-synthesized samples was analyzed by using powder X-ray diffraction (XRD, STOE STADI P) with Mo Kα radiation (wavelength of 0.7093 Å). The oxygen and nitrogen contents of the synthesized samples were determined by hot gas extraction using a Leco TC436 analyzer. Fourier Transform Infrared (FT-IR) spectroscopy was performed on a Varian 670-IR spectrometer. Thermogravimetric analysis (TGA 92, SETARAM) under an ammonia atmosphere was performed to obtain the weight change of samples. A high resolution transmission electron microscope (HRTEM, JEOL JEM-2100F) was used to assess the morphology and the local crystallinity of the samples.

High temperature oxidative-solution calorimetry was used to determine the enthalpies of formation of the prepared oxynitride samples. This method is well developed[15–18] and has been applied previously to study nitrides[19–21] and oxynitrides.[22–24] Using this technique, ~5 mg pellets, prepared by pressing the powders into a die with a diameter of 1 mm, were dropped from room temperature into molten sodium molybdate ($3Na_2O{\cdot}4MoO_3$) solvent at 701 °C using a custom made Tian–Calvet twin microcalorimeter.[15,17]

Neutron diffraction (ND) experiments were performed using a high resolution powder diffractometer for thermal neutrons (HRPT)[25] located at the Swiss Spallation Neutron Source (SINQ) of the Paul Scherrer Institute in Switzerland and the Fine Resolution Powder Diffractometer (FIREPOD, E9)[26] at the BERII of the Helmholtz-Zentrum Berlin (HZB), Germany. The measurements were performed using a neutron wavelength of λ = 1.494 Å at SINQ and λ = 1.308 Å at HZB. Crystallographic parameters were confirmed by the individual Rietveld refinements of the XRD and ND patterns. The peak shapes were modeled with the pseudo-Voigt function for XRD and the Thompson-Cox-Hastings pseudo-Voigt function[27] for ND patterns. Isotropic thermal parameters of O/N were constrained to the same value for the anions. All refinements were performed with the Fullprof software.[28]

3 Results and discussion

3.1 Ammonolysis of scheelite-type oxides

3.1.1 $BaMoO_4$ and $BaWO_4$. The ammonolysis of the scheelite-type $BaMoO_4$ was performed at 600, 700 and 900 °C for 6 h. The sample treated at 600 °C already formed small amounts of the $Ba_3Mo_2(O,N)_8$ oxynitride phase (structure identical to $Ba_3Mo_2N_6N_2$ [29,30]), as shown in Fig. S1.† At 700 °C, Mo_3N_2 [31] and $BaMoO_3$ [32] were observed. Up to 900 °C, only small amounts of Mo_3N_2 were detected besides the main phase $Ba_3Mo_2(O,N)_8$. The absence of the perovskite-type $BaMo(O,N)_3$ is consistent with the experimental work of Liu *et al.*[12] and our previousprediction.[9] The crystallographic data and phase compositions of the samples obtained at 700 and 900 °C were analyzed by Rietveld refinement (Fig. S2a and b†). The refined lattice parameter of $BaMoO_3$ was 4.0489 (6) Å, which is similar to reported values.[11,33] No cubic perovskite $BaMo(O,N)_3$ was formed. The lattice parameters of the rhombohedral $Ba_3Mo_2(O,N)_8$ were 5.9670 (3) and 21.4812 (10) Å (Table S1†); these values are smaller than those of $Ba_3Mo_2O_6N_2$ (5.9706 (5) and 21.5020 (6) Å)[34] probably because of the lower nitrogen content in our as-synthesized oxynitrides (however, we balanced eqn (1)–(3) based on $Ba_3Mo_2O_6N_2$ and $Ba_3W_2O_6N_2$).

A noticeable reaction between $BaWO_4$ and NH_3 occurs at 700 °C (Fig. S3†). Compared to $BaMoO_4$, $BaWO_4$ seems to be rather more inert against ammonia, thus more than 50 wt% of $BaWO_4$ still remained after ammonolysis at temperatures up to 850 °C (Table S2†). Hence, the ammonolysis of $BaWO_4$ at 700 and 850 °C leads to a mixture consisting of $BaWO_4$, $Ba_3W_2(O,N)_8$ and $W_{4.6}N_4$. The lattice parameters of $Ba_3W_2(O,N)_8$ and $W_{4.6}N_4$ assessed by Rietveld refinement of the XRD patterns (Fig. S4†) are close to those reported in ref. 29 and 34 (see also the ESI, Tables S2 and S4†). As we recently predicted,[9] the perovskite-type $BaWO_2N$ cannot be formed.

The samples obtained upon ammonolysis of $BaMoO_4$ and $BaWO_4$ were also investigated by FTIR spectroscopy; both show an absorption band around 975 cm^{-1} for oxynitride (Fig. S5†), which was assigned to a stretching mode (ν(M–N)) in $(WO_3N)^{3-}/(MoO_3N)^{3-}$, having W^{6+}/Mo^{6+} in tetrahedral coordination, as reported by Herle *et al.*[30]

Thus ammonolysis of the scheelite-type oxides $BaWO_4$ and $BaMoO_4$ leads to non-perovskite oxynitride products following the paths proposed in eqn (1)–(3):

$$10BaMoO_4 + \frac{38}{3}NH_3 \overset{700\,^{\circ}C}{\Rightarrow} 3Ba_3Mo_2(O,N)_8 + BaMoO_3 + Mo_3N_2 + 19H_2O + \frac{14}{3}N_2 \quad (1)$$

$$9BaMoO_4 + 12NH_3 \overset{900\,^{\circ}C}{\Rightarrow} 3Ba_3Mo_2(O,N)_8 + Mo_3N_2 + 18H_2O + 2N_2 \quad (2)$$

$$69BaWO_4 + 92NH_3 \overset{850\,^{\circ}C}{\Rightarrow} 23Ba_3W_2(O,N)_8 + 5W_{4.6}N_4 + 138H_2O + 13N_2 \quad (3)$$

3.1.2 $SrMoO_4$ and $SrWO_4$. A similar ammonolysis procedure was applied to the scheelite-type $SrMoO_4$ and $SrWO_4$.

XRD measurements confirm that the ammonolysis of $SrMoO_4$ at 700 °C for 4 h leads to the formation of $SrMoO_2N$ (Fig. 1). The change of the O/N ratio with annealing time in $SrMoO_2N$ was shown to decrease from 2.3 upon annealing time of 4 h (the empirical chemical composition of the oxynitride $SrMoO_{2.09(1)}N_{0.91(1)}$) to 1.89 after 12 h ($SrMoO_{1.96(1)}N_{1.04(1)}$) and to 1.54 after 24 h of ammonolysis ($SrMoO_{1.82(1)}N_{1.18(1)}$). However, the nitrogen incorporation seems to have limitations under the conditions used, thus nitrogen-rich compositions (*e.g.*, $SrMoON_2$, with an O/N ratio of 0.5) are not accessible in this way.

The ammonolysis of scheelite-type $SrWO_4$ at 900 °C leads to the corresponding perovskite-type oxynitride as well (Fig. 2). However, the temperature required to obtain phase-pure Sr,W-based oxynitrides was higher than that used for $SrMoO_4$. The nitrogen content of the $SrW(O,N)_3$ increases slightly with the increasing temperature and holding time. Moreover, the O/N ratio in $SrW(O,N)_3$ seems to be more constant than that in $SrMo(O,N)_3$ and appears to be independent of the annealing time. Thus, the O/N ratio decreases only slightly as the annealing time was extended from 4 h ($SrWO_{1.50(6)}N_{1.50(6)}$; O/N ratio 1.08) to 12 h ($SrWO_{1.42(2)}N_{1.58(2)}$; O/N ratio 0.98) and to 24 h ($SrWO_{1.39(2)}N_{1.61(2)}$; O/N ratio 0.86). Interestingly, the Sr,W-based system can accommodate more nitrogen than its analogous Sr,Mo-based system. Nevertheless the O/N ratio still cannot be pushed down to 0.5.

3.1.3 $CaMoO_4$ and $CaWO_4$. The ammonolysis of $CaMoO_4$ was found to proceed in a different way, leading to the formation of CaO and various molybdenum nitrides (including Mo_2N, Mo_3N_2 and MoN, depending on the temperature, time and ammonia flow) (Fig. S6†) and consequently $CaMoO_4$ was not considered further as a precursor for the corresponding perovskite-type oxynitrides.

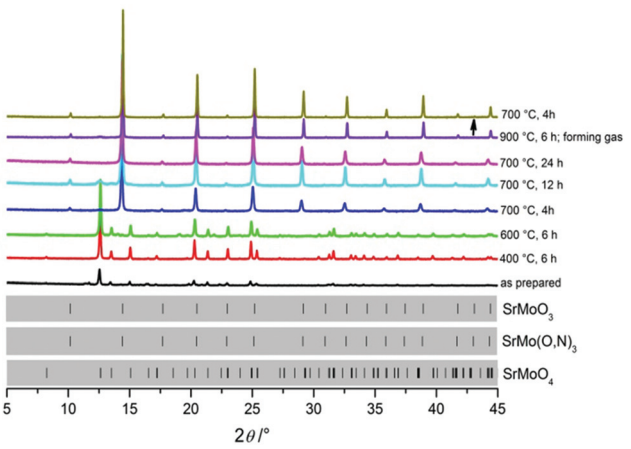

Fig. 1 XRD patterns of $SrMoO_4$ after heating at 400, 600 and 700 °C for different times under an ammonia flow in forming gas (a mixture of 5 vol% H_2 and 95 vol% N_2). The arrow indicates the diffraction pattern of the oxynitride obtained upon ammonolysis of $SrMoO_3$ which was synthesized by reducing $SrMoO_4$ under an ammonia flow at 700 °C.

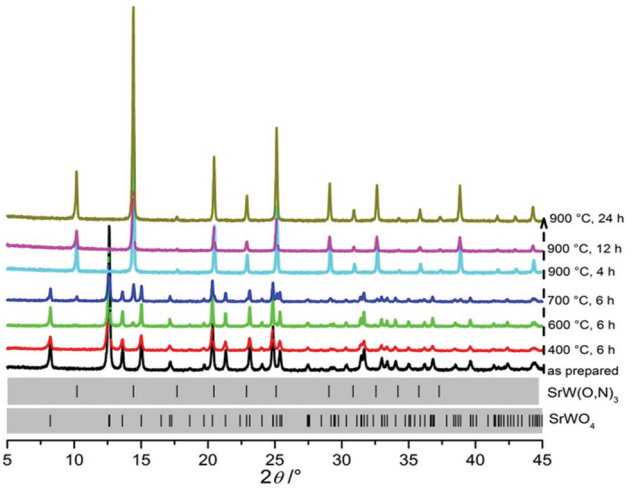

Fig. 2 XRD patterns of $SrWO_4$ after heating at 400, 600, 700 and 900 °C for different times under an ammonia flow.

Ammonolysis of $CaWO_4$ at 900 °C for 6 h leads to complete decomposition into Ca_3WO_6 and $W_{4.6}N_4$ and no oxynitride phase was observed (Fig. S6†). For both $CaMoO_4$ and $CaWO_4$, the corresponding perovskite oxynitrides did not form and thus their conversion into an oxide/nitride mixture is assumed to occur as follows:

$$6CaMoO_4 + 12NH_3 \xrightarrow{700\,^\circ C} 6CaO + Mo_2N + Mo_3N_2 + MoN + 18H_2O + 4N_2 \quad (4)$$

$$6.9CaWO_4 + 9.2NH_3 \xrightarrow{900\,^\circ C} 11.5Ca_3WO_6 + W_{4.6}N_4 + 13.8H_2O + 2.6N_2 \quad (5)$$

3.2 Intermediate oxynitride phase during the conversion of $SrMoO_4$ into perovskite-type $SrMoO_2N$

An interesting phenomenon during the ammonolysis of $SrMoO_4$ at 600 °C relates to the incorporation of 2.23 wt% nitrogen without the formation of any new crystalline phase; thus, the color of the sample changed from white to light-grayish and the FTIR spectrum showed a new absorption band at 978 cm^{-1} related to $(MoO_3N)^{3-}$ units in tetrahedral coordination (Fig. 3a),[30] as also observed in $Ba_3Mo_2(O,N)_8$. Tetracoordinated Mo^{6+} in scheelite-type $SrMoO_4$ can be identified by FTIR spectroscopy *via* a very broad band around 822 cm^{-1} representing the antisymmetric stretching vibrations of Mo–O in $(MoO_4)^{2-}$ tetrahedral units.[35] Thus, the formation of $(MoO_3N)^{3-}$ is considered to be a result of the substitution of one oxygen with nitrogen in $(MoO_4)^{2-}$ tetrahedra. Therefore, we assume that an intermediate scheelite-type oxynitride phase $SrMoO_{4-x}N_x$ (x = 0.39 in our experiment, as obtained from elemental analysis and Rietveld refinement, Fig. 4) forms at 600 °C, which subsequently rearranges into the perovskite structure while taking up more nitrogen. The absence of the absorption band of $(MoO_3N)^{3-}$ in the samples obtained upon

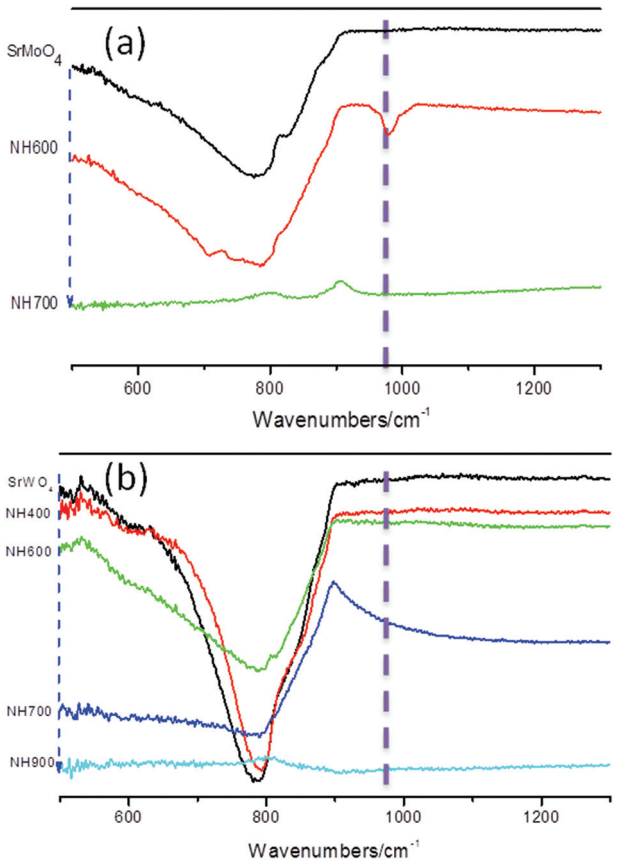

Fig. 3 FTIR spectrum of the as-synthesized scheelite oxide: (a) $SrMoO_4$, (b) $SrWO_4$ and the resulting oxynitrides from ammonolysis at different temperatures (400, 600, 700 and 900 °C) for 6 h.

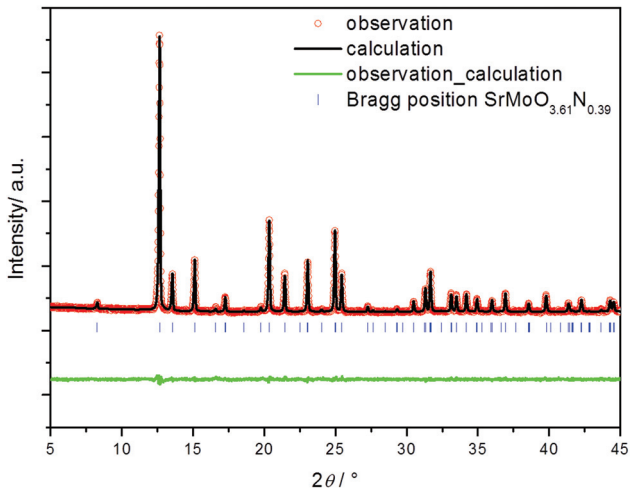

Fig. 4 Rietveld patterns of the X-ray powder diffraction data of the sample obtained upon ammonolysis of $SrMoO_4$ at 600 °C for 4 h. Blue tick marks are Bragg peak positions of the related phase $SrMoO_{3.61(3)}N_{0.39(3)}$ (the ratio of O/N was fixed based on the results of the elemental analysis). The green line at the bottom denotes the difference in intensities between the observed and calculated profiles. Table S3† summarizes the results of the structure refinement.

ammonolysis at temperatures above 700 °C might be related to the strong absorption of the black sample.

Yang *et al.*[36] reported the formation of analogous scheelite-type $EuWO_{4-y}N_y$ oxynitride as the intermediate phase during the nitridation from $Eu_2W_2O_9$ to $EuWO_{1+x}N_{2-x}$. However, in their case, the nitrogen substitution is compensated by the partial oxidation of Eu^{2+} to Eu^{3+} (y = 0.04 in $EuWO_{4-y}N_y$; *i.e.*, $Eu^{2+}{}_{1-y}Eu^{3+}{}_yWO_{4-y}N_y$[36,37]). In our system, Sr^{2+} is not able to be oxidized to Sr^{3+}, so a different mechanism must be responsible for the formation of the nitrogen-containing scheelite-based phase. A likely explanation is that the generation of oxygen vacancies compensates the extra negative charge due to the replacement of oxygen by nitrogen within the pre-formed crystallites, which usually occurs for nitrogen-doped TiO_2 [38,39] or HfO_2.[40] As shown in the HRTEM image within the FFT pattern (Fig. 5), the crystalline phase in the sample obtained after ammonolysis of $SrMoO_4$ at 600 °C for 4 h was indexed as tetragonal ($I41/a$, *i.e.* the same as scheelite-type $SrMoO_4$) and exhibited the presence of pores. Some defect regions with different fringe distances were observed as well probably due to the distortion of the lattice. Interestingly, thermogravimetric analysis of the $SrMoO_4$ in ammonia revealed a slight mass increase of the sample at temperatures up to 600 °C (Fig. 6), indicating that the oxygen, which is expected to be released from $SrMoO_4$ upon ammonolysis, might be stored at intermediate temperatures in the pores or interstitially in the structure as molecular oxygen[13] before being released (as shown by the mass loss of $SrMoO_4$ at temperatures beyond 700 °C, see Fig. 6). This was shown to be the reason for anomalous magnetic behavior at T = −219 °C (54 K) as reported by Logvinovich *et al.* The sharp weight loss above 650 °C is attributed to the complete conversion from scheelite to perovksite resulting in 1 mol oxygen release. Elemental analyses confirm the expected oxygen loss for samples heated in NH_3 between 600 and 700 °C and are in agreement with the measured mass loss, indicating that nitrogen is already incorporated into the sample at 600 °C. (Tables 1 and S6†).

Based on all these observations, we conclude that the nitridation of $SrMoO_4$ occurs prior to the reduction of W^{6+} during ammonolysis, thus scheelite-type $SrMoO_{4-x}N_x$ forms as an intermediate phase and decomposes fast according to the following paths (σ stands for the amount of oxygen vacancies):

$$SrMoO_4 + xNH_3 \xrightarrow{\sim 600\,^\circ C} SrMoO_{4-\sigma-x}V_{O\sigma}^{\cdot\cdot}N_x + \left(\frac{\sigma}{2}\right)O_2 + xH_2O + \frac{x}{2}H_2 \quad (6)$$

$$SrMoO_{4-\sigma-x}V_{O\sigma}^{\cdot\cdot}N_x + NH_3 \xrightarrow{>600\,^\circ C} SrMoO_{3-x-y}N_{x+y} + H_2O + H_2 \quad (7)$$

3.3 Ammonolysis of $SrMoO_4$ *vs.* $SrMoO_3$

In order to investigate the influence of the oxide precursor on the final oxynitride, we converted the scheelite-type $SrMoO_4$

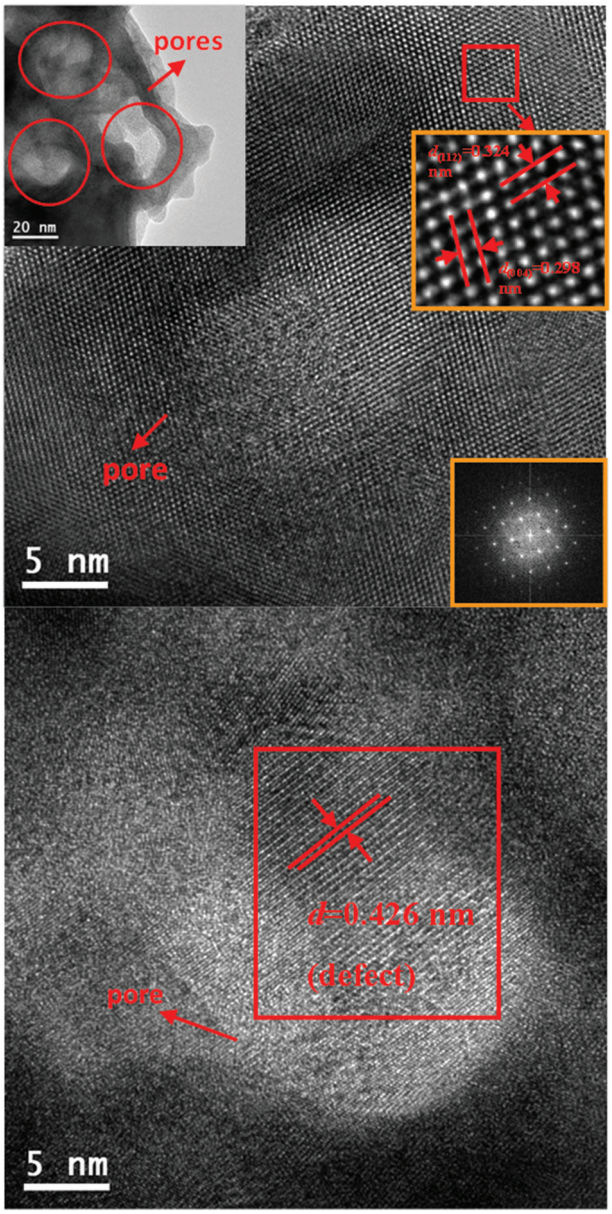

Fig. 5 HRTEM micrographs of $SrMoO_4$ after heating at 600 °C for 4 h.

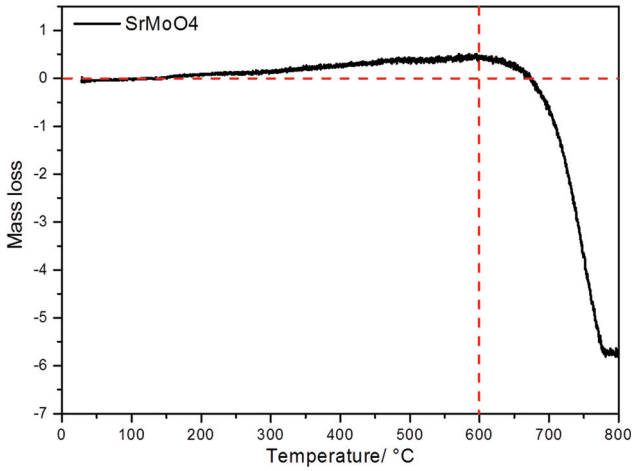

Fig. 6 TG curve of $SrMoO_4$ under an ammonia atmosphere from room temperature to 800 °C.

Table 1 Experimental and calculated mass loss of $SrMoO_4$ upon ammonolysis at 600 and 700 °C. The calculated mass loss relies on the evolution of the chemical composition of the sample upon ammonolysis

Specimens	Experiment	Empirical formula	Calculated
$SrMoO_4$_NH600_4H	0.4218 g	$SrMoO_{3.61}N_{0.39}$	
$SrMoO_4$_NH700_12H	0.3925 g	$SrMoO_{1.96}N_{1.04}$	
Mass loss (wt %)	6.95		6.97

into $SrMo(O,N)_3$ *via* a two-step process as well. In the first step, the scheelite-type oxide $SrMoO_4$ was easily reduced to the perovskite-type $SrMoO_3$ (Fig. S7†) upon thermal annealing at 900 °C for 6 h under forming gas (a mixture of 5 vol% H_2 and 95 vol% N_2). In the subsequent step, $SrMoO_3$ underwent ammonolysis at 700 °C for 4 h (the same conditions as for $SrMoO_4$) to obtain $SrMo(O,N)_3$. Interestingly, the nitrogen content of the phase-pure perovskite-type oxynitride (empirical formula $SrMoO_{2.77(3)}N_{0.23(3)}$, see the Rietveld refinement data of the neutron diffraction pattern shown in Fig. 7a) obtained from perovskite-type $SrMoO_3$ was significantly lower than that of the oxynitride obtained under the same conditions from $SrMoO_4$ ($SrMoO_{2.19(2)}O_{0.81(2)}$). This obviously relates to the oxidation state of Mo in $SrMoO_4$ and $SrMoO_3$ and its evolution under an ammonia atmosphere which will be discussed later.

Moreover, the attempt to synthesize perovskite-type $SrWO_3$ upon reducing $SrWO_4$ at high temperatures was unsuccessful.

3.4 Structural verification of perovskite oxynitrides

The neutron powder diffraction data measured at room temperature for $SrMo(O,N)_3$ and $SrW(O,N)_3$ were refined by the Rietveld method on the basis of the cubic $Pm\bar{3}m$ perovskite-type structure (Fig. 7 and Table 2). The refined O/N content of $SrMoO_{2.19(2)}N_{0.81(2)}$ (700 °C for 4 h) and $SrWO_{1.50(6)}N_{1.50(6)}$ (900 °C for 4 h) is consistent with the results of elemental analysis (ESI, see Table S6†).

The enthalpies of dissolution (ΔH_{ds}) and formation (ΔH_f) of scheelite-type $SrMoO_4$ and $SrWO_4$ and the corresponding perovskite-type oxynitride samples measured by high temperature oxide melt solution calorimetry are listed in Table 3.

The enthalpies of formation of the oxides and oxynitrides from the elements were calculated using the thermodynamic cycles shown in Tables S7 and S8† and are given in Table 3. The enthalpy of formation of $SrMoO_4$ (−260.2 ± 0.5 kJ per g-atom) is ~36 kJ per g-atom more exothermic than that of $SrMoO_{1.96}N_{1.04}$ (−223.8 ± 0.7 kJ per g-atom). Likewise, the enthalpy of formation of $SrWO_4$ (−273.4 ± 0.5 kJ per g-atom) is ~83 kJ per g-atom more exothermic than that of $SrWO_{1.5}N_{1.5}$

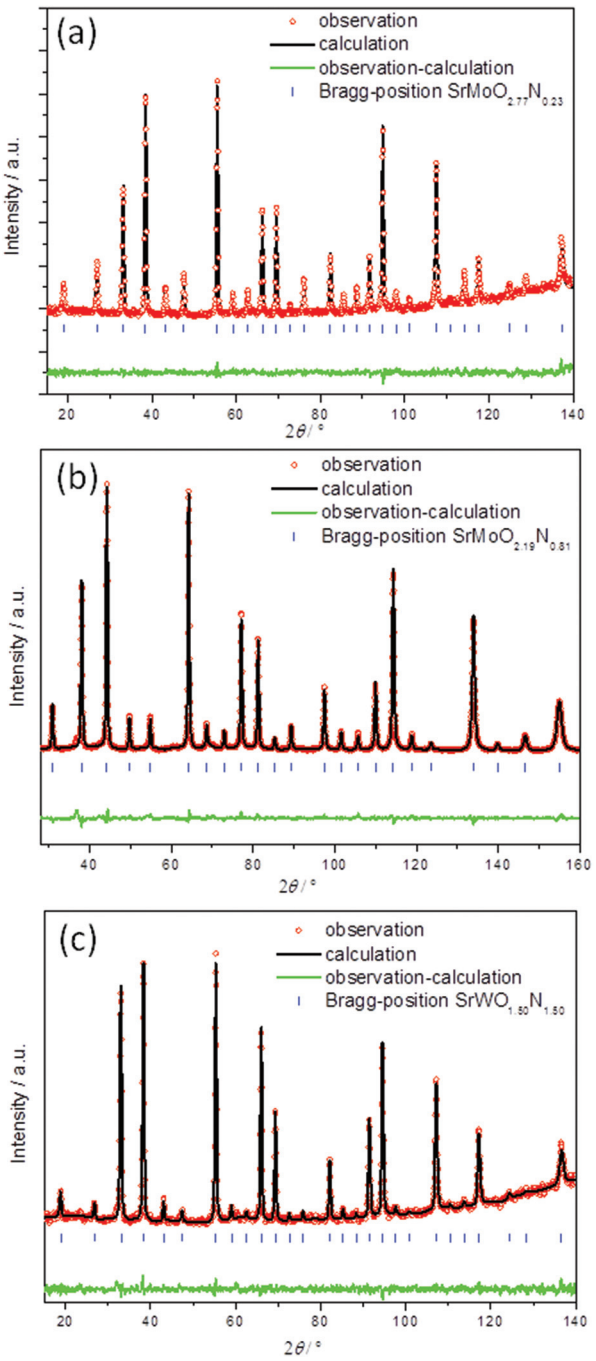

Fig. 7 Rietveld patterns of the neutron powder diffraction data of the sample obtained upon ammonolysis of (a) $SrMoO_3$ at 700 °C for 4 h (FIREPOD, E9); (b) $SrMoO_4$ at 700 °C for 4 h (HRPT, SINQ) and (c) $SrWO_4$ at 900 °C for 4 h (FIREPOD, E9). Blue tick marks are Bragg peak positions of related phases (a) $SrMoO_{2.77(3)}N_{0.23(3)}$; (b) $SrMoO_{2.19(2)}N_{0.81(2)}$ and (c) $SrWO_{1.50(6)}N_{1.50(6)}$. The green line at the bottom denotes the difference in intensities between the observed and calculated profiles.

(−190.4 ± 0.7 kJ per g-atom). Thus, perovskite-type oxynitrides show less favorable enthalpies of formation than their corresponding scheelite-type oxides. Furthermore, the difference of the enthalpy of formation for Sr–W is larger than that of Sr–Mo. This suggests that the formation of Sr–W oxynitrides is less favorable and requires higher temperatures (as observed), probably for both thermodynamic and kinetic reasons.

In order to gain further insights into the energetics of the conversion of $SrMO_4$ into $SrM(O,N)_3$ (M = Mo, W) under an ammonia atmosphere, the Gibbs free energy (ΔG) of reactions (8) and (9) was calculated (Tables S9 and S10†). Since the entropies of $SrMoO_2N$ and $SrWO_{1.5}N_{1.5}$ are not available, we estimated them as 5/6 of the entropy of the corresponding scheelite-type oxide. Eqn (9) and (11) describe the temperature evolution of the Gibbs free energy of the reaction of $SrMO_4$ with NH_3 to give $SrM(O,N)_3$, indicating that the reaction is spontaneous at temperatures exceeding 992 K (*i.e.*, 719. °C) for $SrWO_4$, whereas for $SrMoO_4$ the reaction seems to be thermodynamically favorable at any of the temperatures used for its ammonolysis (Fig. 8). It is worth pointing out that only a thermodynamic consideration might not be enough to describe the ammonolysis processes of the scheelite oxides. The kinetics (*e.g.*, activation energy) of the ammonolysis probably also play an important role and thus might explain why the conversion of $SrMoO_4$ into the perovskite oxynitride needs temperatures exceeding 600 °C and proceeds through an intermediate phase.

$$SrMoO_4 + 2NH_3 = SrMoO_2N + 2H_2O + H_2 + \frac{1}{2}N_2 \quad (8)$$

$$\Delta G_{Sr\text{–}Mo}\ (\text{kJ mol}^{-1}) = 50.404 - 0.197T \quad (9)$$

$$SrWO_4 + 2NH_3 = SrWO_{1.5}N_{1.5} + \frac{5}{2}H_2O + \frac{1}{2}H_2 + \frac{1}{4}N_2 \quad (10)$$

$$\Delta G_{Sr\text{–}W}\ (\text{kJ mol}^{-1}) = 175.615 - 0.177T \quad (11)$$

The negative temperature dependence of the free energy reflects positive entropy of the reaction because 1.5 moles of gas are produced.

3.5 Factors affecting the formation of perovskite-type oxynitrides

As addressed above, the experimental results related to the conversion of $BaMoO_4$, $BaWO_4$, $SrMoO_4$ and $SrWO_4$ into perovskite-type oxynitrides are consistent with our prediction.[9] However, $CaMoO_4$ and $CaWO_4$ do not appear to be converted to oxynitrides.

Scheelite-type ABO_4 oxides are rather common precursors for the synthesis of perovskite oxynitrides, *e.g.* $Nd^{3+}V^{4+}O_2N$,[41] $Eu^{2+}Nb^{5+}O_2N$[5], $La^{3+}Nb^{4+}O_2N$,[42] $Ca^{2+}{}_xSr^{2+}{}_{1-x}W^{5+}O_2N$[43] and so on. The formation of hydrogen due to the dissociation of ammonia at high temperatures is beneficial for the reduction of the B-site cation in scheelite-type oxides (*e.g.* from $A^{2+}B^{6+}O_4$ to $A^{2+}B^{5+}O_2N$ or from $A^{3+}B^{5+}O_4$ to $A^{3+}B^{4+}O_2N$). In the case of using perovskite oxides as precursors for perovskite-type oxynitrides, the B-site cation has to be oxidized in order to compensate for the increase of the negative charge resulting from nitrogen incorporation (*e.g.* from $Sr^{2+}Mo^{4+}O_3$ to $Sr^{2+}Mo^{5+}O_2N$). Thus, it seems that scheelite-type oxide precursors are more favorable for the synthesis of perovskite-type oxynitrides.

Table 2 Crystal structure data of $AB(O,N)_3$ perovskite oxynitrides

	Specimens and parameters	$SrMoO_{2.77(3)}N_{0.23(3)}$	$SrMoO_{2.19(2)}N_{0.81(2)}$	$SrWO_{1.50(6)}N_{1.50(6)}$
S.G.		$Pm\bar{3}m$, Nr. 221	$Pm\bar{3}m$, Nr. 221	$Pm\bar{3}m$, Nr. 221
Z		1	1	1
a,b,c (Å)		3.9744(3)	3.9756(1)	3.9856(2)
Sr	x,y,z	0.5, 0.5, 0.5	0.5, 0.5, 0.5	0.5,0.5, 0.5
	B_{iso} (Å^2)	0.666(25)	0.879(21)	0.738(56)
	Occ.	1	1	1
Mo/W	x,y,z	0.0, 0.0, 0.0	0.0, 0.0, 0.0	0.0, 0.0, 0.0
	B_{iso} (Å^2)	0.298(23)	0.693(18)	0.880(57)
	Occ.	1	1	1
O/N	x,y,z	0.5, 0.0, 0.0	0.5, 0.0, 0.0	0.5, 0.0, 0.0
	B_{iso} (Å^2)	0.748(18)	0.799(12)	0.798(32)
	Occ.	2.77(3)/0.23(3)	2.19(2)/0.81(2)	1.50(6)/1.50(6)

Table 3 Thermochemical data obtained by drop-solution calorimetry of scheelite-type oxides and their corresponding perovskite-type oxynitrides

Composition	Crystal structure	ΔH_{ds} (kJ mol^{-1})	ΔH_f (kJ mol^{-1})	ΔH_f (kJ per g-atom)
$SrMoO_4$	Tetragonal/scheelite	161.8 ± 1.5	−1561.3 ± 3.1	−260.2 ± 0.5
$SrMoO_{1.96}N_{1.04}$	Cubic/perovskite	−291.9 ± 2.3	−1119.1 ± 3.6	−223.8 ± 0.7
$SrWO_4$	Tetragonal/scheelite	−162.8 ± 1.5	−1641.2 ± 3.1	−273.4 ± 0.5
$SrWO_{1.5}N_{1.5}$	Cubic/perovskite	−537.2 ± 1.9	−952.9 ± 3.6	−190.4 ± 0.7

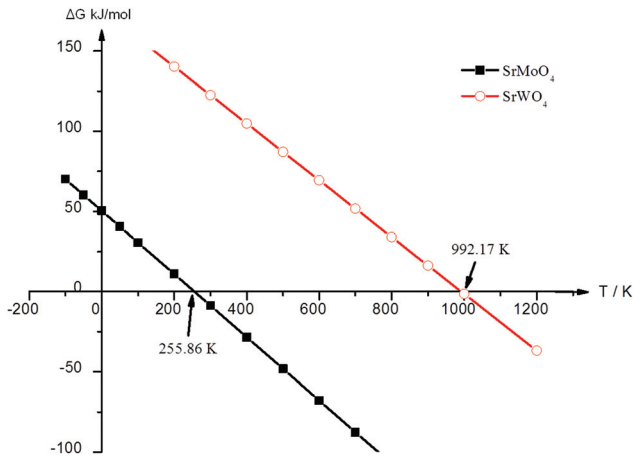

Fig. 8 Gibbs free energy (ΔG) for the ammonolysis of $SrMoO_4$ and $SrWO_4$ (eqn (8) and (10), respectively) as a function of temperature.

Moreover, parameters such as the tolerance factor (describing the distortion of the cubic perovskite structure) were shown to be crucial for the formability of perovskite-type oxynitrides.[9] As defined by Goldschmidt,[44] the tolerance factor (t) in ABX_3 is expressed as:

$$t_O = \frac{(r_A - r_X)}{\sqrt{2}(r_B - r_X)} \quad (12)$$

r_A, r_B and r_X being the ionic radii of A, B and X atoms, respectively.

In our previous work,[9] the formability of perovskite-type oxynitrides was also rationalized upon assessing the values of the tolerance factor, defined as in eqn (13) (see Table 4, as for the O/N ratio 2, *i.e.* ABO_2N):

$$t_{oxy} = \frac{[(r_A + r_O)^8 \times (r_A + r_N)^4]^{1/12}}{\sqrt{2}[(r_B + r_O)^4 \times (r_B + r_N)^2]^{1/6}} \quad (13)$$

For a general consideration of the formability of perovskite-type oxynitrides, we compared their tolerance factors with those of the corresponding perovskite-type oxides. The values of the tolerance factors t_o and t_{oxy} calculated from the ionic radii[45] are shown in Table 4 and indicate that the formal substitution of O^{2-} with N^{3-} in $SrMoO_3$, $SrWO_3$, $CaMoO_3$ and $CaWO_3$ reduces the structural distortion (*i.e.*, the tolerance factor becomes closer to unity), which suggests that the formation of the corresponding perovskite-type oxynitrides is favorable. This is in agreement with the experiment for Sr–Mo/Sr–W compounds and does not fit the experimental observations for Ca–Mo/Ca–W compositions. Large basic cations like Ca typically stabilize higher oxidation states of the transition metals (Mo, W as in our case),[46,47] thus this may explain why the Ca scheelite-type oxides cannot be converted into oxynitrides.

In contrast, incorporation of nitrogen into $BaMoO_3$ and $BaWO_3$ increases the structural distortion; thus, the formation of $BaMoO_2N$ and $BaWO_2N$ would be less favorable. This is in agreement with our synthetic observation.

Moreover, the higher covalent character of the B-site-N bond than that of the B-site-O bond might also induce structural distortion into the perovskite structure of oxynitrides as

Table 4 The tolerance factors for ABO_3 and ABO_2N calculated with eqn (12) and (13), respectively[a]

Oxide	$BaMoO_3$	$BaWO_3$	$SrMoO_3$	$SrWO_3$	$CaMoO_3$	$CaWO_3$
t_O	1.03	1.027	0.98	0.975	0.945	0.941
t_{oxy}	1.053	1.048	0.995	0.989	0.959	0.955
Oxynitride	$BaMoO_2N$	$BaWO_2N$	$SrMoO_2N$	$SrWO_2N$	$CaMoO_2N$	$CaWO_2N$
Predicted[b,9]	N	N	P	P	P	P
Experiment[c]	N	N	P	P	P[11]	N

[a] P: perovskite; N: non-perovskite. [b] The predicted formability of oxynitrides. [c] The formability of oxynitrides for this work.

compared to their analogous perovskite oxides, *i.e.* $B(O,N)_6$ octahedra are expected to be more distorted than their analogous BO_6 octahedra. This structural distortion might be quite pronounced, as for compounds which exhibit so-called second-order Jahn–Teller distortion[48] (*i.e.* d^0 B-site octahedra such as in $LaZrO_2N$, $NdTiO_2N$ or $LaTiO_2N$).[4] However, we consider in our compound $SrM(O,N)_3$ the first-order Jahn–Teller effect is relevant and thus the contribution of the B-site-N covalency to the distortion might not be significant.

4 Conclusions

In the present study, preparative possibilities to access perovskite-type oxynitrides $AM(O,N)_3$ (A = Ba, Sr, Ca; B = Mo, W) phases upon thermal ammonolysis of scheelite-type AMO_4 oxide precursors were investigated. The as-synthesized results of perovskite-oxynitrides are consistent with our previous prediction in general.

The experimental data reveal that both scheelite-type $SrMoO_4$ and $SrWO_4$ transform into a scheelite-type oxynitride intermediate phase, $SrMO_{4-x}N_x$ (M = Mo, W), which subsequently converts fast into perovskite-type $SrM(O,N)_3$ at temperatures above 600 °C and are in agreement with the high temperature oxide melt solution calorimetry experiments which indicate that the conversion of scheelite $SrMO_4$ into perovskite $SrM(O,N)_3$ is thermodynamically favorable at the ammonolysis temperatures used.

Furthermore, the formability of the perovskite-type oxynitrides depends on the structure of the oxide precursor used (scheelite seems to be favorable, except for large basic A cations) and on the structural distortion described by the tolerance factor.

Acknowledgements

The authors acknowledge Dr Samuel Bernard (IEM, University Montpellier 2) for the TGA of $SrMoO_4$ under an ammonia atmosphere. This work was supported by Dr Denis Sheptyakov and based on experiments performed at the Swiss Spallation Neutron Source (SINQ), Paul Scherrer Institute, Villigen, Switzerland. This research was funded by the European Union Seventh Framework Programme (FP7/2007–2013) under the grant agreement FUNEA – Functional Nitrides for Energy Applications. The calorimetry at UC Davis was supported by the U.S. Dept. of Energy, Office of Basic Energy Sciences, grant DE-FG02-03ER46053.

Notes and references

1 A. Fuertes, *J. Mater. Chem.*, 2012, **22**, 3293–3299.
2 Y. I. Kim and P. M. Woodward, *J. Solid State Chem.*, 2007, **180**, 3224–3233.
3 S. G. Ebbinghaus, H. P. Abicht, R. Dronskowski, T. Müller, A. Reller and A. Weidenkaff, *Prog. Solid State Chem.*, 2009, **37**, 173–205.
4 S. J. Clarke, B. P. Guinot, C. W. Michie, M. J. C. Calmont and M. J. Rosseinsky, *Chem. Mater.*, 2002, **14**, 288–294.
5 A. B. Jorge, J. Oró-Solé, A. M. Bea, N. Mufti, T. T. M. Palstra, J. A. Rodgers, J. P. Attfield and A. Fuertes, *J. Am. Chem. Soc.*, 2008, **130**, 12572–12573.
6 D. Logvinovich, R. Aguiar, R. Robert, M. Trottmann, S. G. Ebbinghaus, A. Reller and A. Weidenkaff, *J. Solid State Chem.*, 2007, **180**, 2649–2654.
7 P. Maillard, F. Tessier, E. Orhan, F. Chevire and R. Marchand, *Chem. Mater.*, 2005, **17**, 152–156.
8 F. Chevire, F. Tessier and R. Marchand, *Mater. Res. Bull.*, 2004, **39**, 1091–1101.
9 W. J. Li, E. Ionescu, R. Riedel and A. Gurlo, *J. Mater. Chem. A*, 2013, **1**, 12239–12245.
10 Y. I. Kim, P. M. Woodward, K. Z. Baba-Kishi and C. W. Tai, *Chem. Mater.*, 2004, **16**, 1267–1276.
11 D. Logvinovich, M. H. Aguirre, J. Hejtmanek, R. Aguiar, S. G. Ebbinghaus, A. Reller and A. Weidenkaff, *J. Solid State Chem.*, 2008, **181**, 2243–2249.
12 G. Liu, X. H. Zhao and H. A. Eick, *J. Alloys Compd.*, 1992, **187**, 145–156.
13 D. Logvinovich, J. Hejtmanek, K. Knizek, M. Marysko, N. Homazava, P. Tomes, R. Aguiar, S. G. Ebbinghaus, A. Reller and A. Weidenkaff, *J. Appl. Phys.*, 2009, **105**, 023522.
14 R. M. Po Antoine, Y. Lament, C. Michel and B. Raveau, *Mater. Res. Bull.*, 1988, **23**, 953–957.
15 A. Navrotsky, *Phys. Chem. Miner.*, 1977, **2**, 89–104.
16 J. M. McHale, G. R. Kowach, A. Navrotsky and F. J. DiSalvo, *Chem. – Eur. J.*, 1996, **2**, 1514–1517.

17 A. Navrotsky, *Phys. Chem. Miner.*, 1997, **24**, 222–241.
18 A. Navrotsky, *J. Alloys Compd.*, 2001, **321**, 300–306.
19 S. H. Elder, F. J. Disalvo, L. Topor and A. Navrotsky, *Chem. Mater.*, 1993, **5**, 1545–1553.
20 M. R. Ranade, F. Tessier, A. Navrotsky, V. J. Leppert, S. H. Risbud, F. J. DiSalvo and C. M. Balkas, *J. Phys. Chem. B*, 2000, **104**, 4060–4063.
21 M. R. Ranade, F. Tessier, A. Navrotsky and R. Marchand, *J. Mater. Res.*, 2001, **16**, 2824–2831.
22 J. J. Liang, A. Navrotsky, V. J. Leppert, M. J. Paskowitz, S. H. Risbud, T. Ludwig, H. J. Seifert, F. Aldinger and M. Mitomo, *J. Mater. Res.*, 1999, **14**, 4630–4636.
23 F. Tessier and A. Navrotsky, *Chem. Mater.*, 2000, **12**, 148–154.
24 I. Molodetsky, A. Navrotsky, F. DiSalvo and M. Lerch, *J. Mater. Res.*, 2000, **15**, 2558–2570.
25 P. Fischer, G. Frey, M. Koch, M. Konnecke, V. Pomjakushin, J. Schefer, R. Thut, N. Schlumpf, R. Burge, U. Greuter, S. Bondt and E. Berruyer, *Physica B*, 2000, **276**, 146–147.
26 D. M. Tobbens, N. Stusser, K. Knorr, H. M. Mayer and G. Lampert, *Epdic 7: European Powder Diffraction, Pts 1 and 2*, 2001, **378–3**, 288–293.
27 P. Thompson, D. E. Cox and J. B. Hastings, *J. Appl. Crystallogr.*, 1987, **20**, 79–83.
28 J. Rodriguezcarvajal, *Physica B*, 1993, **192**, 55–69.
29 Z. G. Pinsker, *Acta Crystallogr.*, 1957, **10**, 775–775.
30 P. S. Herle, M. S. Hegde and G. N. Subbanna, *J. Mater. Chem.*, 1997, **7**, 2121–2125.
31 V. V. Klechkovskaya, N. V. Troitskaya and Z. G. Pinsker, *Sov. Phys. Crystallogr. (Engl. Transl.)*, 1965, **10**, 28–35.
32 R. Scholder and L. Brixner, *Z. Naturforsch., B: Chem. Sci.*, 1955, **10**, 178–179.
33 L. H. Brixner, *J. Inorg. Nucl. Chem.*, 1960, **14**, 225–230.
34 M. T. Weller and S. J. Skinner, *Int. J. Inorg. Mater.*, 2000, **2**, 463–467.
35 A. P. A. Marques, M. T. S. Tanaka, E. Longo, E. R. Leite and I. L. V. Rosa, *J. Fluoresc.*, 2011, **21**, 893–899.
36 M. Yang, J. Oro-Sole, A. Kusmartseva, A. Fuertes and J. P. Attfield, *J. Am. Chem. Soc.*, 2010, **132**, 4822–4829.
37 A. Kusmartseva, M. Yang, J. Oró-Solé, A. M. Bea, A. Fuertes and J. P. Attfield, *Appl. Phys. Lett.*, 2009, **95**, 02210.
38 J. B. Varley, A. Janotti and C. G. Van de Walle, *Adv. Mater.*, 2011, **23**, 2343–2347.
39 A. K. Rumaiz, J. C. Woicik, E. Cockayne, H. Y. Lin, G. H. Jaffari and S. I. Shah, *Appl. Phys. Lett.*, 2009, 95.
40 M. Yang, J. H. Bae, C. W. Yang, A. Benayad and H. Baik, *J. Anal. Atom. Spectrom.*, 2013, **28**, 482–487.
41 J. Oró-Solé, L. Clark, W. Bonin, J. P. Attfield and A. Fuertes, *Chem. Commun.*, 2013, **49**, 2430–2432.
42 D. Logvinovich, S. C. Ebbinghaus, A. Reller, I. Marozau, D. Ferri and A. Weidenkaff, *Z. Anorg. Allg. Chem.*, 2010, **636**, 905–912.
43 Y. Masatomo, F. Uhi, N. Hiromi, O. Kazuki and R. H. James, *J. Phys. Chem. C*, 2013, **117**, 18529–18539.
44 V. M. Goldschmidt, *Skrifer Norske Videnskaps-Akad*, I. Mat. Naturv., Oslo, 1926.
45 R. D. Shannon and C. T. Prewitt, *Acta Crystallogr., Sect. B: Struct. Crystallogr. Cryst. Chem.*, 1969, **25**, 925–946.
46 K. Kamata, T. Nakamura and T. Sata, *Chem. Lett.*, 1975, 81–86.
47 K. Kamata, T. Nakamura and T. Sata, *Mater. Res. Bull.*, 1975, **10**, 373–378.
48 R. G. Pearson, *Proc. Natl. Acad. Sci. U. S. A.*, 1975, **72**, 2104–2106.